Antitumor Polycyclic Acridines. 17.[1] Synthesis and Pharmaceutical Profiles of Pentacyclic Acridinium Salts Designed To Destabilize Telomeric Integrity

Jennifer C. Cookson, Robert A. Heald, and Malcolm F. G. Stevens*

Cancer Research U.K. Experimental Cancer Chemotherapy Research Group, Centre for Biomolecular Sciences, School of Pharmacy, University of Nottingham, Nottingham NG7 2RD, U.K.

Received June 1, 2005

Palladium(0)-mediated Suzuki−Miyaura and Heck transformations have been exploited to provide examples of 8-methylquino[4,3,2-*kl*]acridines and 8,13-dimethylquino[4,3,2-*kl*]acridinium iodides bearing bulky saturated (3-acetoxy)propyl or (*E*)-3-(morpholin-4-yl)-3-oxopropenyl substituents variously in the 3-, 6-, or 10-positions of the pentacyclic nucleus. The pharmacological/pharmaceutical properties of four compounds (**4**, RHPS4), (**5**, IH383), (**6**, RHPS16), and (**17**, RHPS19) were measured to assess their clinical potential as DNA G-quadruplex-stabilizing/telomerase inhibitory agents. The following properties were measured: stability in tissue culture media in the presence of A549 lung and MCF-7 breast tumor cells, metabolic stability when incubated with rat liver microsomes, and rate of uptake and subcellular location in A549 and MCF-7 cells. Compound **17** was unstable in tissue culture media, failed to achieve nuclear access, and was excluded from further consideration. Of the other agents, **4** exhibited the most favorable pharmaceutical profile: the agent has appropriate stability in the presence of tumor cells and rat liver microsomes and achieves rapid ingress into cell nuclei where the putative molecular target is located.

Introduction

In recent papers in this series, we have described new syntheses[2] and biological activities[3−5] of derivatives of the DNA-affinic 8*H*-quino[4,3,2-*kl*]acridine skeleton **1** (Chart 1), work that was inspired by reports of the pharmacological properties of related polycyclic acridines of marine[6] or fungal[7] origin. Of particular interest were derivatives of the 8,13-dimethylquinoacridinium pharmacophore (e.g., **2**), which differ in the electronic nature of substituents appended to the three benzo rings.[5] Of the first-generation compounds, **3** (RHPS3), with electron-donating methyl substituents, is potently growth-inhibitory to human cancer cell lines, has a COMPARE profile[8] typical of a topoisomerase II inhibitor, and binds promiscuously to duplex DNA and higher-ordered DNA polymorphs. In contrast (**4**, RHPS4), with electron-withdrawing fluoro substituents in the 3- and 11-positions, has a higher affinity for triplex and quadruplex DNA and is only weakly growth-inhibitory overall to tumor cells. Both **3** and **4** inhibit telomerase in the TRAP assay with $^{tel}IC_{50} < 0.35\ \mu M$.[5] The ability of **4** to bind to, and stabilize, G-quadruplex structures formed from the single-stranded hexanucleotide telomeric repeat $(TTAGGG)_n$ has been confirmed by high-field NMR studies.[9] Recently, we have expanded the scope of our synthetic chemistry to develop routes to second-generation heteroaromatic salts such as substituted aminoquinoacridinium salts exemplified by **5** (IH383), which has a biological fingerprint in the NCI 60 cell assay different from that of **4**.[10]

On the basis of our recent NMR investigations[9] and guided by results from Read et al. on a related series of G-quadruplex-binding 3,6-disubstituted-9-anilinoacridines,[11] we theorized that molecules with substituents in significant positions on the quinoacridinium pharmacophore (e.g. 3-, 6-, and 10) (see Figure 1) might have enhanced affinity for maintaining G-quadruplex structures through augmented binding within the quadruplex grooves. An example of the latter type is the pentacyclic acridinium salt (**6**, RHPS16) with a 3-acryloylmorpholinyl substituent.[2] Such compounds have the potential to exert antitumor activity by disrupting telomere maintenance (capping)[12] and/or denying telomerase enzyme the single-stranded DNA sequence required as its substrate.[13]

Ideally an attractive clinical candidate selected from this class of agent should have the following design characteristics: (i) ease of synthesis, (ii) a unique

Chart 1. Numbering Scheme for the 8*H*-Quino[4,3,2-*kl*]acridine Ring System (**1**) and Structures of Bioactive 8,13-Dimethylquinoacridinium Salts (**2**−**6**)

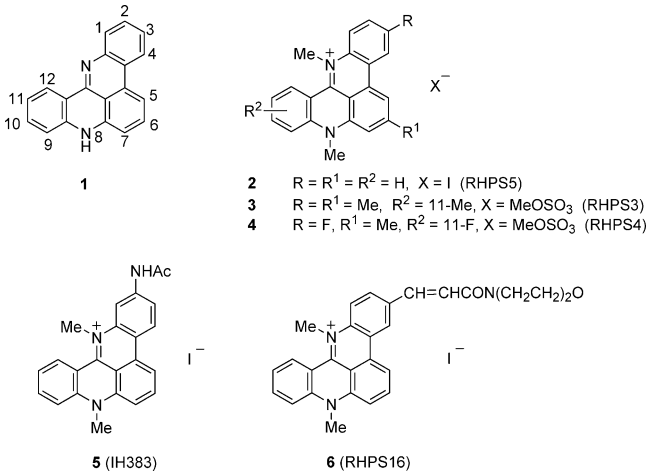

* To whom correspondence should be addressed. Phone: (115) 951 3414. Fax: (115) 951 3412. E-mail: malcolm.stevens@nottingham.ac.uk.

10.1021/jm058031y CCC: $30.25
Published on Web 10/15/2005

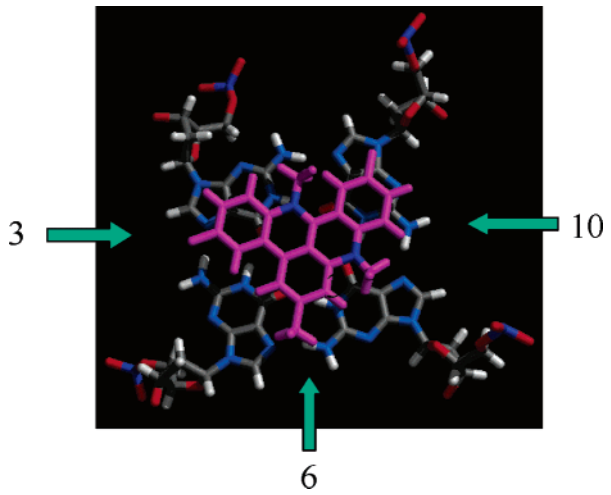

Figure 1. Model of the binding of **4** to a parallel-stranded d(TTAGGGT)$_4$ quadruplex as a view down the long axis showing the 3-, 6-, and 10-positions of the pentacyclic nucleus (ref 9). Compound **4** is colored in magenta, and the nitrogen atoms of the guanine bases are in blue.

biological profile consequent on disorganizing a molecular target not yet evaluated in the clinic, and (iii) robust and exploitable pharmaceutical qualities. In this work we have not exploited any specific molecular modeling considerations in the choice of substituents in the 3-, 6-, or 10-positions that might enhance binding to G-quadruplex structures; rather, we have focused on exploring the applicability of palladium(0)-mediated methodology to secure synthetic access to 8,13-dimethylquinoacridinium salts with potentially fragile peripheral substituents. Because of synthetic availability and stability issues, three 8,13-dimethylquinoacridinium salts embellished with appended "druglike" substituents were selected for pharmaceutical profiling in comparison with the previously synthesized pentacycle (**4**).[5]

Results and Discussion

Chemistry. A combination of palladium(0)-mediated Suzuki−Miyaura and Heck reactions can be used to decorate the quino[4,3,2-*kl*]acridine skeleton, with Heck chemistry being notably high-yielding. Thus, we have shown previously that the borane **7**, prepared in situ from 9-borabicyclo[3,3,1]nonane (9-BBN) and allyl acetate, couples with the triflate-substituted 8-methylacridines **8** and **9** in the presence of $Pd(OAc)_2$ catalyst and PPh_3 ligand and Cs_2CO_3 base at 150 °C to furnish the 6-(3-acetoxypropyl)-substituted acridines **10** and **11** in 60% and 63% yields, respectively.[2] We now show that, even in the presence of this potentially fragile ester moiety, chloroquinoacridines **10** and **11** will undergo a second palladium(0)-catalyzed Suzuki−Miyaura reaction with borane **7** to give the 3,6-disubstituted **12** and 6,10-disubstituted **13** products but in only 13% and 20% yields (Scheme 1). Rewardingly more efficient was a Heck reaction of the 3-chloroquinoacridine **10** and 4-acryloylmorpholine in the presence of a $Pd_2(dba)_3$ catalyst and P(*t*-Bu)$_3$ ligand at 170 °C for 48 h to afford the 3,6-disubstituted quinoacridine **14** (83%). Neutral 8-methylquinoacridines **12**−**14** were then processed to the required dimethylquinoacridinium salts **15**−**17** with methyl iodide at 100 °C. More salts (**18**−**24**) with a range of unsaturated side chains in the 3-, 6-, or 10-positions were prepared similarly by methylation of previously reported precusor 8-methylquinoacridines[2] (see Table 1 for structures).

Telomerase Inhibition and Growth Inhibitory Characteristics of 8,13-Dimethylquinoacridinium Salts in Vitro. Results of evaluation of compounds as telomerase inhibitors (TRAP assay) and in growth inhibition assays (NCI mean GI_{50} values) are recorded in Table 1. Partial results for compounds **18**−**24** are included. The unsubstituted pentacyclic salt **2** has an $^{tel}IC_{50}$ of 0.38 μM, and compounds with a single substituted alkenyl group variously in the 3-, 6-, and 10- (or 11-) positions, and the 2-acetylamino-quinoacridinium salt **5**), are approximately equipotent in the TRAP assay. Compounds incorporating two substituted alkyl groups (3-acetoxypropyl) in the 3,6-positions (**15**) or 6,10-positions (**16**) and the monosubstituted propionic acid ester **23** are approximately 10-fold less potent.

Although incorporating single or multiple bulky substituents onto the pentacyclic scaffold disappointingly brings no gain in telomerase inhibitory potency, such variations strikingly modulate growth-inhibitory activities as measured by mean GI_{50} values in the NCI 60 human tumor cell panel.[14] Within the limited series of compounds fully evaluated for telomerase inhibition and in vitro growth-inhibitory properties, compounds bearing a 3-acryloylmorpholinyl group (**6** and **17**) have low mean GI_{50} values with methiodide salt **6** having the highest selectivity index (SI = (mean GI_{50})/($^{tel}IC_{50}$) = 183) (Table 1). In other preliminary work we have attributed this desirable outcome to reduced affinity of **6** for duplex DNA, which correlates to cytotoxicity.[15] Four compounds (**4**−**6** and **17**) with the most favorable SIs were selected for broader pharmacological profiling.

Physical Properties of 8,13-Dimethylquinoacridinium Salts. The most water-soluble compound was the difluoroquinoacridinium methosulfate **4**, which would afford a stable 5 mM aqueous solution (>2 mg/mL) at 25 °C. Compounds with an acryloylmorpholinyl substituent in the 3-position (**6** and **17**) were the least soluble of the analogues; at room temperature 500 μM aqueous solutions could be achieved but precipitation occurred at 1 mM. Amide **5** was between **4** and **6** with a limit to aqueous solubility between 1 and 5 mM at 25 °C. With the exception of compound **17**, compounds had molecular weights (cationic species only) less than 450 and log *P* values (calculated)[16] less than 4 in compliance with Lipinski's "rule of five".[17] Although the dimethylquinoacridinium cation is formally represented with positive charge located on N-13 (**25**), charge can be delocalized on N-8 (**25a**) and the cation could be depicted more accurately as the resonance-stabilized structure **25b** (Scheme 2); electron-donating substituents (X, Y, Z) in the peripheral rings (e.g., Me, OMe) would reduce the overall electron deficiency of the pentacyclic core, whereas electron-withdrawing groups (e.g., F, Cl) would augment the deficiency. These features might modulate the ability of pentacyclic acridinium salts to act as surrogate potassium ions and stabilize DNA quadruplex structures.[13]

Drug Stability in the Presence of A549 (Lung) and MCF-7 (Breast) Human Tumor Cells. The three salts (**4**−**6**) were stable at 37 °C in RPMI tissue culture medium (including 10% FBS) alone. Incubation of 10

Scheme 1[a]

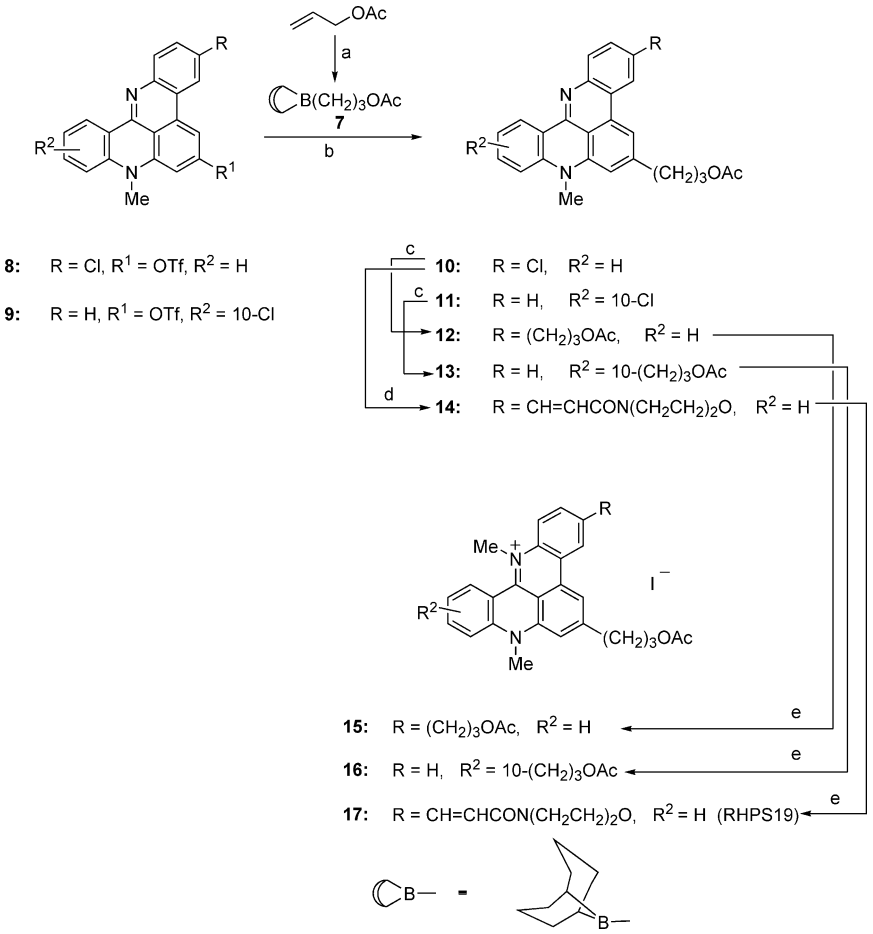

[a] Reagents and conditions: (a) allyl acetate, 9-BBN, THF, 25 °C; (b) ref 2; (c) **7** with **10** or **11**, $Pd_2(dba)_3$, P(*t*-Bu)$_3$, Cs_2CO_3, dioxane, 150 °C, 18 h; (d) **10**, $Pd_2(dba)_3$, P(*t*-Bu)$_3$, K_3PO_4, 4-acryloylmorpholine, 170 °C, 48 h; (e) MeI, 100 °C, 48 h.

Table 1. Biological Properties of Quinoacridinium Salts

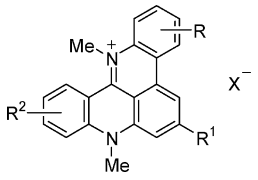

compd	R	R[1]	R[2]	X	$^{tel}IC_{50}$ [a] (μM)	mean GI_{50} [b] (μM)	SI [c]
2	H	H	H	I	0.38	1.29	3.4
3	3-Me	Me	11-Me	$MeOSO_3$	0.25	0.41	1.8
4	3-F	Me	11-F	$MeOSO_3$	0.33	13.18	40
5	2-NHAc	H	H	I	0.38	12.0	31.6
6	3-CH=CHCON$(CH_2CH_2)_2$O	H	H	I	0.37	68	183
15	3-$(CH_2)_3$OAc	$(CH_2)_3$OAc	H	I	3.22	3.80	1.2
16	H	$(CH_2)_3$OAc	10-$(CH_2)_3$OAc	I	2.30	3.31	1.45
17	3-CH=CHCON$(CH_2CH_2)_2$O	$(CH_2)_3$OAc	H	I	0.38	27.5	72.4
18	H	OMe	10-CH=$CHCO_2$Me	I	>1.0	4.58	
19	H	OMe	10-CH=CHCON$(CH_2CH_2)_2$O	I	2.18	43.7	2.0
20	H	OMe	10-CH=CHCON$(CH_2CH_2)_2$NAc	I		93.3	
21	3-Cl	CH=CHCON$(CH_2CH_2)_2$O		I		12.0	
22	3-CH=$CHCO_2$Me	H		I	0.2		
23	3-$(CH_2)_2CO_2$Me	H		I	3.02		
24	3-CH=CHCON$(CH_2CH_2)_2$O	OMe		I		9.33	

[a] TRAP assay (refs 4 and 5). [b] In the NCI 60 cell panel (ref 14). [c] Selectivity index: mean $GI_{50}/^{tel}IC_{50}$.

μM solutions over 72 h did not result in any loss of absorbance at λ_{max} wavelengths or change the shape of the absorbance spectrum (data not shown). Compound **17** was unstable in this environment (see below). Incubations of drugs (0.5 μM) with A549 or MCF-7 cells, followed by HPLC analysis of aliquots of the culture medium, gave information on drug stability in the presence of cells, in vitro.

The persistence of salts **4**−**6** in culture medium with A549 cells over a 72 h incubation period was determined by HPLC analysis (Figure 2). Slight diminution of the peak heights of **5** and **6** was observed (final peak areas

Scheme 2

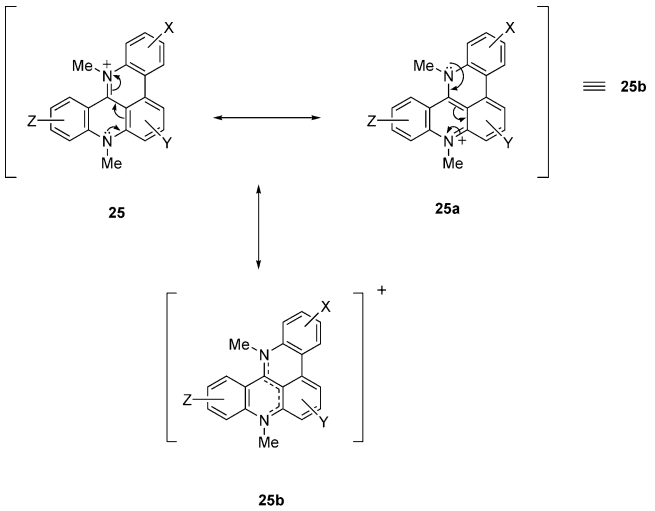

are approximately 90% of time zero value), but there was no detectable loss of salt **4**. Intriguingly, the results in MCF-7 cells were different, notably with amide **5**, which showed a 43% depletion in peak height after 72 h. The mechanism for this degradation is unknown but possibly involves a metabolic process in MCF-7 cells that is absent in A549 cells, the steady reduction in peak height in a linear fashion suggesting an intrinsic pathway as opposed to an induced one. Representative HPLC traces showing the stability of **5** in the presence of A549 and MCF-7 cells at time zero and after 72 h are included in Supporting Information.

The 3,6-disubstituted quinoacridinium salt **17** was unstable in tissue culture media at 37 °C. HPLC analysis of aliquots of the drug solution (10 μM) in culture medium alone showed loss of parent compound accompanied by the appearance of a more polar secondary peak. After 48 h of incubation, there were approximately equal proportions of each species (see Supporting Information). An LC−MS analysis of the 72 h sample in culture medium showed an ion at 494 corresponding to $\mathbf{17}^+ - 42$ (CH_2=C=O). Thus, this contaminant is tentatively identified as the alcohol **26** formed by hydrolytic deacetylation of **17** (Scheme 3).

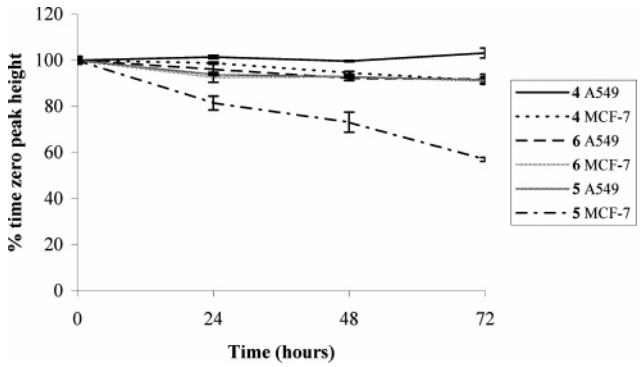

Figure 2. Stability of **4**−**6** (0.5 μM) in tissue culture medium containing 10% fetal bovine serum, incubated with A549 or MCF-7 cells (37 °C, 5% CO_2, humidified atmosphere) over 72 h. The height of the drug peak as a percentage of the time zero value is shown as the mean value (and standard deviation) of two flasks. Results were reproducible in similar repeat experiments.

Scheme 3[a]

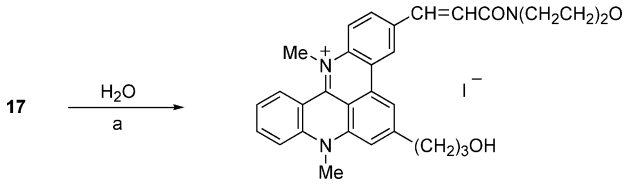

[a] Reagents and conditions: tissue culture medium, 37 °C.

Insufficient material was available to evaluate the biological and pharmaceutical properties of **26**.

Metabolic Stability of Pentacyclic Acridinium Salts in the Presence of Cytochrome P450 Enzymes. Cytochrome P450 enzymes play an important role in metabolizing anticancer agents and thus influence pharmacokinetics, therapeutic effects, and toxicity of drug therapy. Cell lines of the NCI 60 human tumor panel, including A549 and MCF-7, express unique P450 expression patterns albeit at constituitively low basal levels.[18] Moreover, there are examples of drugs *inducing* the expression of a metabolic enzyme. For example, the novel aminoflavone (5-amino-2,3-difluorophenyl)-6,8-difluoro-7-methyl-4*H*-1-benzopyran-4-one induces its own metabolic activation to a cytotoxic DNA-damaging species via CYP1A1/1A2 induction, directly in tumor cells.[19] Also, the antitumor benzothiazole 2-(4-amino-3-methylphenyl)benzothiazole (DF 203) induces CYP1A1 activity in sensitive cell lines only, to undergo 6-hydroxylation to an inactive metabolite.[20]

The vulnerability of pentacyclic acridinium salts **4**−**6** to metabolism by cytochrome P450 enzymes should give insights into how stable the drugs are likely to be to phase 1 metabolism. Possible metabolic pathways envisaged could include N-dealkylation, aryl oxidation, methyl oxidation, or amide cleavage. The microsomes purchased were membrane fractions derived from the liver tissue of a pool of 15 male Sprague-Dawley rats that possess the following spectrum of catalytic activity: 7-ethoxyresorufin *O*-deethylase (CYP1A), *p*-nitrophenol hydroxylase (CYP2E1), testosterone 6β-hydroxylase (CYP3A), testosterone 16α-hydroxylase (CYP2C), lauric acid 12-hydroxylase (CYP4A), cytochrome *c* reductase, and cytochrome b5.

Drugs were incubated with microsomes in buffer solution at 37 °C using a fixed protein content, and after sample preparation, the resulting mixtures were analyzed by HPLC with appropriate blanks. All three drugs tested showed reduction of the parent peak (**4**, 81% remaining after 4 h; **5**, 69%; **6**, 66%) and the appearance of more than one minor peak, representing unknown metabolites, which differed in elution time and therefore identity between the drugs. To control for loss of the parent peak attributable to protein binding (of the microsomes), additional incubations were performed using a control microsome product derived from a human lymphoblast cell line that possesses no detectable cytochrome P450 activity. The control microsomal incubations revealed that protein binding was not the explanation for the reduction in parent compound. Results for the least stable compound (**6**) are shown in Figure 3. The drug DF 203 was used as a positive control for microsomal activity.[20] Near total loss of this compound was noted when incubated with the microsomes (data not shown). The results show that of the three salts

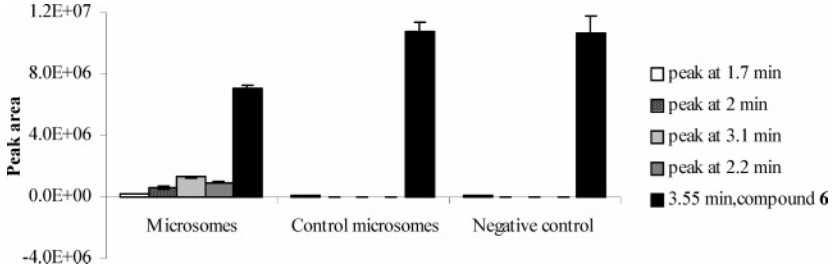

Figure 3. Metabolism of **6** (2 μM) by rat liver microsomes at 37 °C for 4 h. Elution times and areas of the resulting peaks are shown. The results are the mean and standard deviation of three independent experiments, and each experiment was performed in duplicate with mean values calculated.

examined the difluoropentacyclic salt (**4**) is the most metabolically robust agent under these conditions.

Flow Cytometric Assessment of Drug Uptake. Uncharged, small molecules (e.g., drug molecules of molecular weight less than 1000) will diffuse into cells along a concentration gradient; membrane permeability is directly proportional to the lipid solubility of the molecule.[21] For molecules of equivalent polarity, their ability to cross the membrane is inversely proportional to molecular size.[22] Ionized molecules can traverse the gut membrane by combining with a counterion to form an ion pair that behaves as a neutral structure with a high partition coefficient and an ability to cross membranes. Quaternary ammonium compounds are thought to be absorbed in this way.[22] In the case of the pentacyclic acridinium salts, because delocalized charge over the central core of the pentacyclic system is surrounded by hydrophobic phenyl rings, these compounds are soluble in both aqueous and organic media and their amphiphilic nature facilitates rapid uptake into cells.

We have previously employed flow cytometry to track the uptake of **4** into A549 and MCF-7 cells. Uptake was rapid and approached saturation at 2 h in A549 cells or 5 h in MCF-7 cells.[5] In the present work uptake curves for **5** and **6** are shown (Figure 4). The reduced rate and extent of drug uptake at the lower temperature of 4 °C are consistent with reduced diffusion through the lipid bilayer because of decreased membrane fluidity. It is not possible to rule out a facilitated diffusion mechanism wherein energy is expended because carrier proteins with substrate specificity increase the diffusion rate of molecules such as sugars, amino acids, and purines along the concentration gradient. Such a mechanism, like diffusion, has saturable kinetics.[22] No attempt was made to use flow cytometry quantitatively because this would have required a means of relating fluorescence values from cells to drug concentrations. Moreover, the agents vary in intrinsic fluorescence intensity and exhibit unique absorbance and emission wavelength maxima, thus requiring the use of different fluorescence channels. The cells also exhibited a low level of autofluorescence. The shapes of the curves of fluorescence increase, reflecting the time scale of uptake, were consistent for each drug in repeated experiments, as were the magnitudes of the differential between fluorescence values at 4 °C and 37 °C.

The overall pattern of uptake of salt **6** (Figure 4) suggested a less rapid and more gradual accumulation within cells than with **4** and **5**. Cellular incubation with **17** resulted in qualitatively similar results in A549 cells compared to the other analogues but a different uptake profile in MCF-7 cells. In the latter case, absorption was extremely rapid, and maximal fluorescence values at 37 °C, which were reached within 2.5 h, were quantitatively similar to fluorescence at 4 °C, suggesting that the mechanism of cross-membrane transport is different compared to the other polycyclic salts. Moreover, **17**, which has the highest molecular weight of the salts studied, does not gain access to the nucleus (see below), and there is therefore a lower volume of distribution into which diffusion can occur compared to the other agents. The difference in uptake of **17** between the two cell lines may be explained by subtle differences in cell membrane and protein composition.

Intracellular Drug Localization. Confocal laser scanning microscopy was adopted to visualize intracellular distribution of selected pentacyclic acridines in viable cells, exploiting the inherent fluorescent properties of their chromophore. The slice facility of the confocal microscope aids assessment of intracellular drug localization because it allows examination at specific *Z* planes through the cell. Control cells incubated in vehicle but with no drug showed no detectable fluorescence under the experimental conditions (data not shown).

In A549 cells **4** appeared to be localized in the nuclear membrane and intranuclear bodies believed to be the nucleoli (Figure 5a). In MCF-7 this drug conferred a more diffuse pattern of distribution (Figure 5b) with the nuclear membrane, intranuclear bodies, and cytoplasm all staining. A549 and MCF-7 cells incubated with **5** all gave clearly defined images showing dense staining within the nucleus especially at the putative nucleoli and giving an appearance of chromatin staining (parts c and d of Figure 5). In contrast, we observed a heterogeneous pattern of staining by compound **6**. In both A549 and MCF-7 cells (parts e and f of Figure 5) a bright speckled cytoplasmic appearance was obtained with some cells showing discrete bright regions within the nuclei (again, possibly the nucleoli). We interpret these images with some caution because we cannot rule out the possibility of cellular/drug responses to the confocal laser altering the intracellular distribution pattern slightly.

Puzzlingly, the heavily substituted salt **17** deviated in its intracellular distribution from the other featured pentacyclic acridinium salts so far described. Both A549 and MCF-7 cells excluded the agent from the nucleus, though it was incorporated intracellularly, perinuclearly (parts g and h of Figure 5). Again, the bright speckled cytoplasmic appearance was observed, noticeably in A549 cells, with greater intensity immediately surrounding the nucleus than proximal to the cellular membrane. MCF-7 stained less brightly than A549 cells,

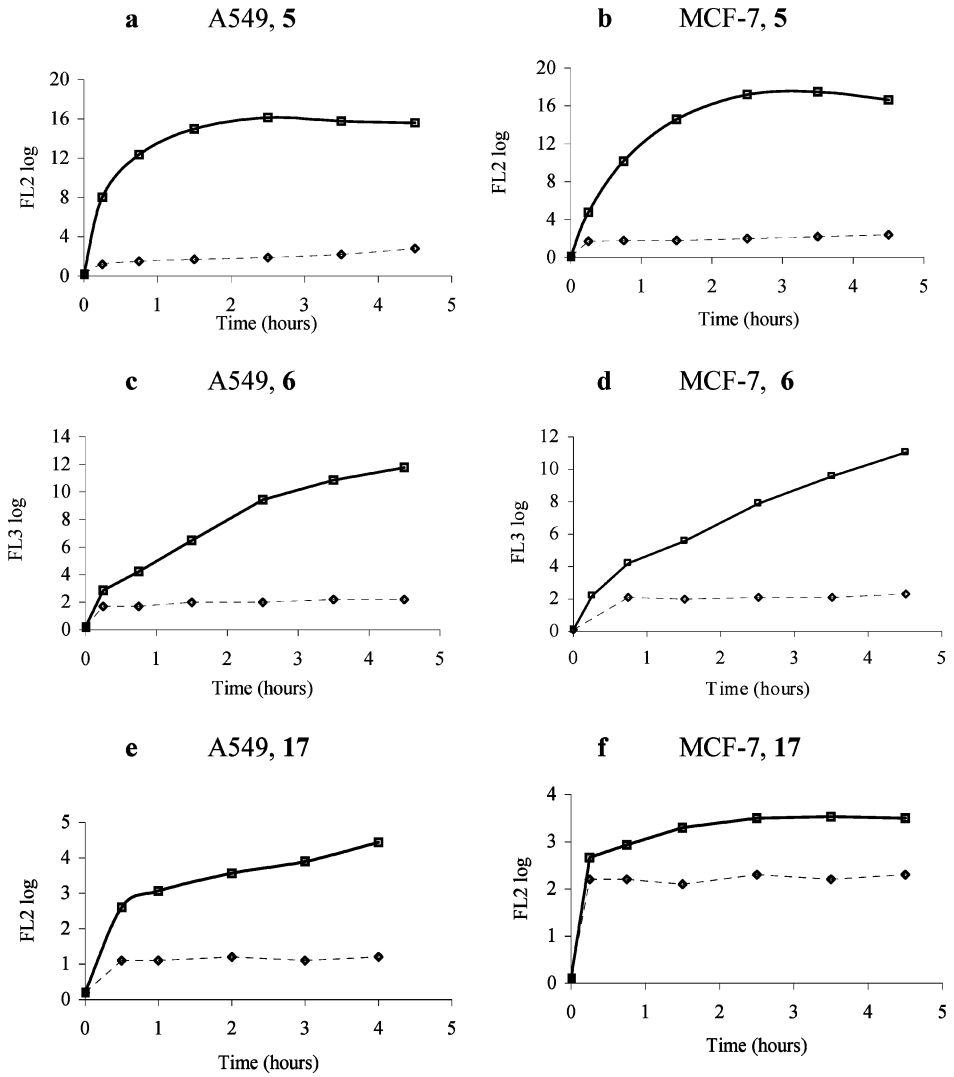

Figure 4. Uptake of **5** (a, b), **6** (c, d), and **17** (e, f) (1 μM for each) into A549 (a, c, e) and MCF-7 (b, d, f) cells at 37 °C (solid lines) or 4 °C (dashed lines). The vertical axis shows the mean fluorescence in the FL2 or FL3 channel (measured on a log scale) of at least 5000 cells. The 37 °C points are the mean of triplicates, and results are representative of at least two independent experiments. Negative controls (incubated without drug) showed no increase in fluorescence (data not shown).

which concurs with the cellular uptake results in which **17** exhibited a particularly rapid but limited uptake pattern in MCF-7 cells compared to A549.

Fluorescent regions within the cytoplasm may be the mitochondria, which are known to take up lipophilic cations and moieties with a delocalized positive charge (e.g., pentacyclic acridinium salts). Differences in membrane potentials between cell lines have been linked to differences in accumulation of lipophilic cations[24] and, in turn, differential cytotoxicity.[25,26] Mitochondria have been observed to selectively accumulate lipophilic cations, while hydrophilic derivatives of the same core structure are distributed widely in cellular compartments.[27] These observations may be applicable to the observed distribution of the pentacyclic acridine analogues, which may be modulated by substituted groups on the pentacyclic core through effects on lipophilicity and charge delocalization/distribution.

The nuclear incorporation of salts **4**−**6** was encouraging because the putative molecular target for the drugs (telomeric DNA) is located in the nuclei. In view of the apparent nucleolar localization of some analogues, it is interesting that the catalytic subunit of the human telomerase enzyme, hTERT, is located predominantly in the nucleolus;[28] the RNA component of human telomerase, hTR, is also localized in the nucleolus by virtue of its box H/ACA motif. It has been reported that the chromosomes appear to have a specific distribution within the nucleus and may be tethered by the telomeres to the nuclear envelope,[23] in which case nuclear membrane localization of the drugs would be expected to result in accessibility to the telomeres. The DNA damage response protein, Ku, is implicated in the localization of telomeres at the nuclear pores,[29] and its presence is required for normal telomere maintenance.[30] In mitosis, the nuclear envelope breaks down, allowing access of cellular organelles to the chromosomes. At this point compound **17**, with telomerase inhibitory potency comparable to that of **4**−**6** in the TRAP assay (Table 1), may gain access to the nuclear contents despite being directly excluded from the nucleus.

Conclusions

Four pentacyclic acridinium salts with varying peripheral substituents were selected for pharmaceutical evaluation on the basis of their synthetic accessibility

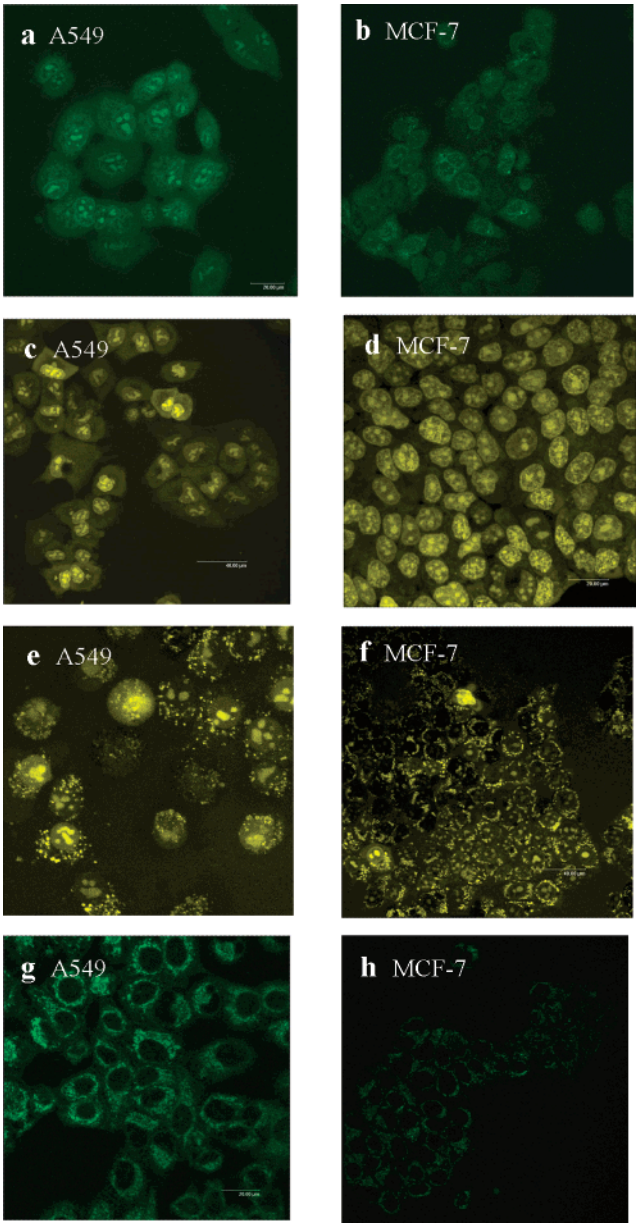

Figure 5. Confocal laser scanning microscopy images of A549 and MCF-7 cells after 24 h of incubation at 37 °C with 20 μM **4** (a, b), **5** (c, d), **6** (e, f), and **17** (g, h). Maximum intensity projections of the slices imaged are shown.

and cellular and biophysical data suggesting they are selective inhibitors of telomerase. The analogues showed workable aqueous solubility and predicted partition coefficients consistent with bioavailability in vivo according to Lipinski's rule of five for molecules to possess druglike properties. With the exception of **17**, the salts showed good stability under the conditions of cell culture, although results in MCF-7 cells with amide **5** suggest that this derivative may be susceptible to cell-type-specific metabolic activity, possibly involving initial hydrolysis. Salts **4**−**6** all showed susceptibility to common phase 1 metabolic transformation with different metabolites for each analogue inferred, the pharmacology of which may become relevant upon in vivo studies.

Rapid cellular uptake of the salts was observed in tumor cell lines (A549 and MCF-7) with the suggestion of a trend to accelerated uptake for the less functionalized molecules. Possible subcellular structures showing particular staining by these intensely fluorescent agents included the nucleoli, nuclear membranes, and possibly mitochondria or other cytoplasmic structures. Membrane structures surrounding organelles and comprising the endoplasmic reticulum may also localize these lipophilic drugs, and the degree of delocalization of positive charge within the series of compounds may be affecting their differential properties. Of the four agents profiled, the difluoroquinoacridinium salt (**4**) shows the most favorable constellation of properties in the series: synthetic accessibility, perturbation of an important new cancer target (telomeric DNA), and robust and potentially exploitable pharmaceutical properties.

Experimental Section

Synthetic Chemistry. Melting points were measured on a Gallenkamp apparatus and are uncorrected. IR spectra were recorded as KBr disks on a Perkin-Elmer Spectrum One FT-IR spectrometer. Mass spectra were recorded on a Micromass Platform spectrometer, an AEI MS-902 (nominal mass), or a VG Micromass 7070E or a Finnigan MAT900 XLT spectrometer (accurate mass). NMR spectra were recorded on a Bruker ARX 250 instrument at 250.13 MHz (^{1}H), 62.9 MHz (^{13}C) in DMSO-d_6 or $CDCl_3$; coupling constants are in Hz. Merck silica gel 60 (40−60 μm) was used for column chromatography.

The following compounds were prepared as referenced: 8,13-dimethyl-8*H*-quino[4,3,2-*kl*]acridinium iodide (**2**),[5] 3,6,8,-11,13-pentamethyl-8*H*-quino[4,3,2-*kl*]acridinium methosulfate (**3**),[5] 3,11-difluoro-6,8,13-trimethyl-8*H*-quino[4,3,2-*kl*]acridinium methosulfate (**4**),[5] 2-acetylamino-8,13-dimethyl-8*H*-quino-[4,3,2-*kl*]acridinium iodide (**5**),[10] 8,13-dimethyl-3-[(*E*)-3-(morpholin-4-yl)-3-oxopropenyl]-8*H*-quino[4,3,2-*kl*]acridinium iodide (**6**), and quinoacridinium iodides (**18**−**24**).[2]

3,6-Di-(3-acetoxypropyl)-8,13-dimethyl-8*H*-quino[4,3,2-*kl*]acridinium iodide (15). Allyl acetate (0.17 mL, 1.55 mmol) and 9-BBN (3 mL of a 0.5 M solution in THF, 2 mol equiv) were stirred at 25 °C for 3.5 h and added to a mixture of 6-(3-acetoxypropyl)-3-chloro-8-methyl-8*H*-quino[4,3,2-*kl*]-acridine (**10**)[2] (0.2 g, 0.05 mmol), $Pd_2(dba)_3$ (4 mol %), P(*t*-Bu)$_3$ (0.05 M in dioxane, 8 mol %), and Cs_2CO_3 (2 mol equiv) in dioxane (5 mL) and heated at 150 °C for 18 h. The cooled mixture was diluted with DCM and chromatographically fractionated on a silica column. Evaporation of the main band afforded crude 3,6-di-(3-acetoxypropyl)-8-methyl-8*H*-quino-[4,3,2-*kl*]acridine (**12**) (13%). Then a mixture of methyl iodide (2 mL) and quinoacridine (**12**, 0.05 g) was heated in a sealed tube at 100 °C for 2 days. Evaporation of excess methyl iodide afforded the quinoacridinium salt **15** (0.035 g, 54%), mp >300 °C (dec). UV (EtOH) λ_{max}, nm: 285, 307, 434, 459. ^{1}H NMR ($CDCl_3$): δ 8.54 (1H, d, J = 7.5 Hz, H-12), 8.29 (1H, s, H-4), 8.12 (2H, m, H-5), 7.79 (2H, m, H-9, H-10), 7.72 (2H, s, H-2, H-7), 7.58 (1H, t, J = 8.5 Hz, H-11), 4.63 (3H, s, N^+CH_3), 4.21 (7H, NCH_3, 2 × CH_2), 3.17 (2H, t, J = 7.5 Hz, CH_2), 2.97 (2H, t, J = 7.5 Hz, CH_2), 2.27 (4H, m, 2 × CH_2), 2.12 (6H, s, 2 × $COCH_3$). ^{13}C NMR ($CDCl_3$): δ 171.5, 152.1, 151.8, 143.8, 141.7, 141.1, 137.7, 136.5, 133.1, 132.5, 130.5, 128.2, 124.1, 123.6, 123.2, 120.2, 117.2, 115.9, 115.4, 115.1, 113.0, 63.9, 63.8, 47.6, 46.4, 37.6, 34.2, 32.4, 30.5, 21.4 (overlapping side chain CO and CH_3 signals). HRMS (FAB) *m/z*: calcd for $C_{31}H_{33}N_2O_4$ (M^+), 497.2440; found, 497.2462.

6,10-Di-(3-acetoxypropyl)-8,13-dimethyl-8*H*-quino[4,3,2-*kl*]acridinium iodide (16). Similarly prepared, from allyl acetate, 9-BBN, 6-(3-acetoxypropyl)-10-chloro-8-methyl-8*H*-quino[4,3,2-*kl*]acridine (**11**)[2], $Pd_2(dba)_3$ (4 mol %), P(*t*-Bu)$_3$ (8 mol % in dioxane), and Cs_2CO_3 in dioxane at 150 °C for 18 h, the quinoacridine **13** was isolated after chromatographic fractionation in 20% yield (eluting solvent 5% MeOH in DCM). Methylation of **13**, as above, with methyl iodide gave the quinoacridinium salt **16** (42%), mp >300 °C (dec). UV (EtOH) λ_{max}, nm: 284, 302, 431, 454. ^{1}H NMR ($CDCl_3$): δ 8.54 (1H, d,

J = 9.0 Hz, H-12), 8.40 (1H, d J = 8.0 Hz, H-4), 8.03 (2H, m, H-1, H-5), 7.76 (1H, t, J = 7.5 Hz, H-2), 7.68 (2H, m, H-7, H-9), 7.61 (1H, t, J = 7.5 Hz, H-3), 7.47 (1H, d, J = 9.0 Hz, H-11), 4.55 (3H, s, N^+CH_3), 4.22 (3H, NCH_3), 4.15 (4H, m, 2 × CH2), 3.10 (2H, t, J = 7.5 Hz, CH_2), 2.95 (2H, t, J = 7.5 Hz, CH_2), 2.23 (4H, m, 2 × CH_2), 2.10 (6H, s, 2 × $COCH_3$). ^{13}C NMR ($CDCl_3$): δ 171.0 (C), 151.6 (C), 151.6 (C), 151.4 (C), 151.3 (C), 143.5 (C), 140.3 (C), 138.6 (C), 132.3 (C), 131.8 (CH), 130.8 (CH), 127.6 (CH), 124.7 (CH), 123.9 (CH), 122.3 (C), 119.3 (CH), 116.0 (CH), 114.9 (C), 114.7 (CH), 113.0 (C), 112.8 (CH), 63.2 (CH_2), 47.0 (CH_3), 37.5 (CH_3), 33.6 (CH_2), 33.0 (CH_2), 30.0 (CH_2), 29.5 (CH_2), 21.0 (overlapping side chain CO and CH_3 signals). HRMS (FAB) *m/z*: calcd for $C_{31}H_{33}N_2O_4$ (M^+), 497.2440; found, 497.2422.

6-(3-Acetoxypropyl)-8,13-dimethyl-3-[(*E*)-3-(morpholin-4-yl)-3-oxopropenyl]-8*H*-quino[4,3,2-*kl*]acridinium Iodide (17). A mixture of 6-(3-acetoxypropyl)-3-chloro-8-methyl-8*H*-quino[4,3,2-*kl*]acridine (**10**)[2] (0.1 g, 0.25 mmol), $Pd_2(dba)_3$ (2 mol %), P(*t*-Bu)$_3$ (0.05 M in dioxane, 8 mol %), K_3PO_4 (2 mol equiv), and 4-acryloylmorpholine (0.07 g, 63 μL, 2 mol equiv) was heated at 170 °C for 48 h in a screw-top tube. To the cooled solution was added DCM, and the suspension was filtered through Celite, with further DCM washing. Chromatographic purification of the mixture on silica (eluting solvent 5% MeOH in DCM) gave the 3,6-disubstituted quinoacridine **14** (0.104 g, 83%). The product was reacted with excess methyl iodide as above to afford the quinoacridinium iodide **17** (0.075 g, 58%), mp 159−161 °C. UV (EtOH) λ_{max}, nm: 285, 448, 476. IR (KBr) ν, cm^{-1}: 1612, 1579, 1450, 1253, 1232, 1113. ^1H NMR ($CDCl_3$): δ 8.68 (1H, d, J = 8.0 Hz, H-12), 8.55 (1H, s, H-5), 8.50 (1H, s, H-4), 7.90 (3H, m, H-1, H-9, H-10), 7.60 (2H, m, H-7, H-11), 7.36 (1H,dd, J = 2.5, 9.5 Hz, H-2), 7.30 (1H, d, J = 15.5 Hz, olefinic CH), 7.11 (1H, d, J = 15.5 Hz, olefinic CH), 4.54 (3H, s, N^+CH_3), 4.21 (2H, t, J = 9.0 Hz, CH_2OAc), 4.18 (3H, NCH_3), 3.70 (8H, m, 4 × CH_2), 3.28 (2H, t, J = 7.6 Hz, CH_2), 2.24 (2H, t, J = 7.5 Hz, CH_2), 2.10 (3H, s, $COCH_3$). ^{13}C NMR ($CDCl_3$): δ 171.2 (C), 165.1 (C), 152.3 (C), 151.6 (C), 143.3 (C), 140.2 (C), 139.9 (CH), 138.9 (C), 136.0 (CH), 134.0 (C), 131.4 (CH), 131.3 (CH), 130.4 (CH), 123.55 (CH), 123.0 (C), 122.8 (CH), 120.1 (CH), 120.0 (CH), 116.7 (CH), 116.6 (CH), 115.2 (C), 114.7 (C), 112.7 (CH), 67.3 (CH_2), 66.9 (CH_2), 63.8 (CH_2), 47.3 (CH_3), 46.0 (CH_2), 42.6 (CH_2), 36.8 (CH_3), 33.5 (CH_2), 30.4 (CH_2), 21.18 (CH_3). HRMS (FAB) *m/z*: calcd for $C_{33}H_{34}N_3O_4$ (M^+), 536.2549; found, 536.2572.

8,13-Dimethyl-6-methoxy-10-[(*E*)-(2-methoxycarbonyl)-vinyl]-8*H*-quino[4,3,2-*kl*]acridinium Iodide (18). Methylation of 8-methyl-6-methoxy-10-[(*E*)-(2-methoxycarbonyl)-vinyl]-8*H*-quino[4,3,2-*kl*]acridine (0.1 g)[2] with methyl iodide (2 mL) at 100 °C for 48 h gave the quinoacridinium iodide **18** (38%), mp 235−237 °C. UV (EtOH) λ_{max}, nm: 316, 341, 374, 483, 503. IR (KBr) ν, cm^{-1}: 1716, 1611, 1578, 1420, 1168. ^1H NMR (DMSO-d_6): δ 8.73 (1H, d, J = 8.0 Hz, H-4), 8.38 (2H, m, H-9, H-12), 8.04 (1H, t, J = 7.0 Hz, H-1), 7.97 (4H, m, H-2, H-5, H-11, olefinic CH), 7.71 (1H, t, J = 7.0 Hz, H-3), 7.36 (1H, s, H-7), 7.11 (1H, d, J = 16.0 Hz, olefinic CH), 4.31 (3H, s, N^+CH_3), 4.17 (3H, s, OCH_3), 4.10 (3H, s, NCH_3). HRMS (FAB) *m/z*: calcd for $C_{26}H_{23}N_2O_3$ (M^+) 411.1709; found, 411.1720.

8,13-Dimethyl-6-methoxy-10-[(*E*)-3-(morpholin-4-yl)-3-oxopropenyl]-8*H*-quino[4,3,2-*kl*]acridinium Iodide (19). Similarly prepared (as above), from 8-methyl-6-methoxy-10-[(*E*)-3-(morpholin-4-yl)-3-oxopropenyl]-8*H*-quino[4,3,2-*kl*]acridine[2] and methyl iodide, the quinoacridinium iodide **19** (64%) had mp 240 °C (dec). UV (EtOH) λ_{max}, nm: 313, 341, 374, 480, 501. IR (KBr) ν, cm^{-1}: 1613, 1578, 1420, 1226, 1137, 1039, 765, 620. ^1H NMR (DMSO-d_6): δ 8.77 (1H, d, J = 7.5 Hz, H-4), 8.42 (1H, m, J = 9.0 Hz, H-12), 8.34 (1H, s, H-9), 8.07 (3H, m, H-1, H-11, olefinic CH), 7.96 (1H, t, J = 7.0 Hz, H-2), 7.90−7.65 (3H, m, H-3, H-5, olefinic CH), 7.40 (1H, s, H-7), 4.35 (3H, s, N^+CH_3), 4.18 (3H, s, OCH_3), 4.15 (3H, s, NCH_3), 3.83 (2H, brs, CH_2), 3.65 (6H, brs, 3 × CH_2). HRMS (FAB) *m/z*: calcd for $C_{29}H_{28}N_3O_3$ (M^+) 46.2131; found, 466.2124.

10-[(*E*)-3-(4-Acetylpiperazin-1-yl)-3-oxopropenyl]-8,13-dimethyl-6-methoxy-8*H*-quino[4,3,2-*kl*]acridinium Iodide (20). Methylation of 10-[3-(4-acetylpiperazin-1-yl)-3-oxopropenyl]-8-methyl-6-methoxy-8*H*-quino[4,3,2-*kl*]acridine (0.25 g)[2] with methyl iodide at 100 °C for 48 h gave the quinoacridinium iodide **20** (0.19 g, 59%), mp >275 °C (dec). UV (EtOH) λ_{max}, nm: 314, 341, 373, 482, 502. IR (KBr) ν, cm^{-1}: 1612, 1579, 1420, 1206, 1034, 997, 762, 659. ^1H NMR (DMSO-d_6): δ 8.79 (1H, d, J = 7.5 Hz, H-4), 8.44 (1H, d, J = 8.5 Hz, H-12), 8.36 (1H, s, H-9), 8.10 (3H, m, H-1, H-11, olefinic CH), 7.94 (1H, t, J = 7.5 Hz, H-2), 7.73 (3H, m, H-3, H-5, olefinic CH), 7.42 (1H, s), 4.36 (3H, s, N^+CH_3), 4.19 (3H, s, OCH_3), 4.16 (3H, s, NCH_3), 3.83 (2H, br s, CH_2), 3.61 (6H, m, 3 × CH_2), 2.09 (3H, s, $COCH_3$). HRMS (FAB) *m/z*: calcd for $C_{31}H_{31}N_4O_3$ (M^+), 507.2396; found, 507.2399.

3-Chloro-8,13-dimethyl-6-[(*E*)-3-(morpholin-4-yl)-3-oxopropenyl]-8*H*-quino[4,3,2-*kl*]acridinium Iodide (21). Prepared (53%) from 3-chloro-8-methyl-6-[(*E*)-3-(morpholin-4-yl)-3-oxopropenyl]-8*H*-quino[4,3,2-*kl*]acridine[2] and methyl iodide (as above), the iodide salt **21** had mp 210 °C (dec). UV (EtOH) λ_{max}, nm: 285, 321, 491, 521. IR (KBr) ν, cm^{-1}: 1580, 1417, 1250, 1114, 1042, 845, 764, 648. ^1H NMR (DMSO-d_6): δ 9.00 (1H, s), 8.89 (1H, s), 8.49 (1H, d, J = 9.0 Hz), 8.37 (1H, s), 8.23−8.14 (3H, m), 8.00−7.92 (3H, m), 7.65 (1H, t, J = 7.0 Hz), 4.37 (3H, s, N^+CH_3), 4.24 (3H, s, NCH_3), 3.90 (2H, br s, CH_2), 3.67 (6H, m, 3 × CH_2). HRMS (FAB) *m/z*: calcd for $C_{28}H_{25}ClN_3O_2$ (M^+), 470.1635; found, 470.1645.

8,13-Dimethyl-3-[(*E*)-(2-methoxycarbonyl)vinyl]-8*H*-quino[4,3,2-*kl*]acridinium Iodide (22). Methylation of 8-methyl-3-[(*E*)-(2-methoxycarbonyl)vinyl]-8*H*-quino[4,3,2-*kl*]-acridine (0.03 g)[2] with methyl iodide (2 mL) at 100 °C for 48 h gave the quinoacridinium iodide **22** (0.025 g, 38%), mp 200−202 °C. UV (EtOH) λ_{max}, nm: 302, 358, 488, 521. IR (KBr) ν, cm^{-1}: 1613, 1584, 1256, 1177, 1096. ^1H NMR (DMSO-d_6): δ 0.10 (1H, s, H-4), 8.66 (1H, d, J = 7.5 Hz, H-12), 8.52 (1H, d, J = 9.5 Hz, H-5), 8.41 (1H, t, J = 8.0 Hz, H-6), 8.23 (1H, t, J = 8.5 Hz, H-10), 8.13 (4H, m, H-1, H-2, H-5, H-9), 7.83 (1H, d, J = 16.0 Hz, olefinic CH), 7.65 (1H, t, J = 7.5 Hz, H-11), 7.04 (1H, d, J = 16.0 Hz, olefinic CH), 4.35 (3H, s, N^+CH_3), 4.21 (3H, s, NCH_3), 3.79 (3H, s, OCH_3). HRMS (ES) *m/z*: calcd for $C_{25}H_{21}N_2O_2$ (M^+) 381.1603; found, 381.1608.

8,13-Dimethyl-3-[(2-methoxycarbonyl)ethyl]-8*H*-quino[4,3,2-*kl*]acridinium Iodide (23). 8-Methyl-3-[(*E*)-(2-methoxycarbonyl)vinyl]-8*H*-quino[4,3,2-*kl*]acridine (0.05 g)[2] was suspended in ethyl acetate (150 mL) and hydrogenated at 40 psi over a 10% palladium/charcoal catalyst (0.1 g) for 48 h. The mixture was filtered through Celite, solvent evaporated, and the residue chromatographically fractionated on a silica column (eluting solvent, 25% EtOAc in hexane). Evaporation of the main band gave impure 8-methyl-3-[(2-methoxycarbonyl)ethyl]-8*H*-quino[4,3,2-*kl*]acridine (0.036 g, 70%). Methylation of a sample (0.03 g) with methyl iodide (2 mL) at 100 °C for 48 h gave the quinoacridinium iodide **23** (0.021 g, 48%), mp 189−191 °C. UV (EtOH) λ_{max}, nm: 251, 307, 440, 460. IR (KBr) ν, cm^{-1}: 2963, 1611, 1437, 1260, 1094, 1024. ^1H NMR (DMSO-d_6): δ 8.67 (1H, s), 8.47 (2H, m), 8.31 (1H, m), 8.10 (4H, m), 7.83 (1H, d, J = 8.0 Hz), 7.63 (1H, d, J = 6.0 Hz), 4.39 (3H, s, N^+CH_3), 4.19 (3H, s, NCH_3), 3.62 (3H, s, OCH_3), 3.15 (2H, t, CH_2), 2.70 (2H, t, CH_2). HRMS (FAB) *m/z*: calcd for $C_{25}H_{23}N_2O_2$ (M^+) 383.1760; found, 383.1762.

8,13-Dimethyl-6-methoxy-3-[(*E*)-3-(morpholin-4-yl)-3-oxopropenyl]-8*H*-quino[4,3,2-*kl*]acridinium Iodide (24). Methylation of 8-methyl-6-methoxy-3-[(*E*)-3-(morpholin-4-yl)-3-oxopropenyl]-8*H*-quino[4,3,2-*kl*]acridine (0.075 g)[2] with methyl iodide (2 mL) at 100 °C for 72 h gave the quinoacridinium iodide **24** (0.07 g, 69%), mp 220 °C (dec). UV (EtOH) λ_{max}, nm: 295, 324, 474, 497. IR (KBr) ν, cm^{-1}: 1608, 1580, 1436, 1225, 1111, 1040, 822, 764. ^1H NMR (DMSO-d_6): δ 9.26 (1H, s, H-4), 8.68 (1H, d, J = 8.0 Hz, H-12), 8.55 (1H, d, J = 8.5 Hz, H-2), 8.44 (1H, s, H-5), 8.39−8.26 (3H, m, H-1, H-9, H-10), 8.03 (1H, d, J = 16.0 Hz, olefinic CH), 7.83−7.77 (2H, m, H-11 and olefinic CH), 7.66 (1H, s, H-7), 4.57 (3H, s, N^+CH_3), 4.42 (3H, s, OCH_3), 4.37 (3H, s, NCH_3), 4.04 (2H, brs, CH_2), 3.85 (6H, brs, 3 × CH_2). HRMS (FAB) *m/z*: calcd for $C_{29}H_{28}N_3O_3$ (M^+) 466.2131; found, 466.2134.

Biological and Pharmaceutical Evaluations. The method for the evaluation of pentacyclic compounds in the Taq

polymerase and TRAP assays followed procedures previously used to assess this class of compound.[4,5] GI_{50} values following a 2-day drug exposure in the in vitro NCI 60 human tumor cell panel were determined according to published methods.[14] Predicted log *P* values were estimated using the interactive "Calculation of Druglikeness" option at http://www.molinspiration.com. Structures were drawn as cations without the counterion in the JME Molecular Editor, a Java applet developed by Ertl et al.[16]

HPLC Assay for Drug Stability in Cell Culture. A549 or MCF-7 cells were seeded into 25 mL [2] flasks (5×10^5 cells/flask) and allowed to attach overnight in RPMI tissue culture medium (10% fetal calf serum) at 37 °C, and then the medium was replaced with drug-containing medium (0.5 μM). The medium was sampled in triplicate at 0, 24, 48, and 72 h, and aliquots were stored at −20 °C until analysis whereupon the aliquots were thawed and diluted with three volumes of acetonitrile to precipitate proteins, then centrifuged at 17000*g* to pellet debris. The supernatant was filtered (0.2 μm PVDF filter, Millex-GV) and analyzed on a Beckman System Gold HPLC operated with 32Karat software using an octadecylsilane (ODS) reversed-phase HPLC column (Hypersil 5 μm C18, 150 mm × 3.2 mm). The mobile phase comprised 65% acetonitrile and 35% aqueous buffer (20 mM potassium dihydrogen orthophosphate and phosphoric acid at pH 2.5, in HPLC-grade water). Triethylamine was included at 0.1% in the aqueous component (before pH adjustment) to reduce peak tailing. The column was equilibrated with mobile phase (65:35 ratio of organic to aqueous components, 0.5 mL/min flow rate) for 45 min before sample injection/chromatography began. A 12 min isocratic run was performed for each sample with fluorescence detection at an excitation wavelength of 483 nm and an emission wavelength of 543 nm.

Incubation of Pentacyclic Acridines with Rat Liver Microsomes. The method was developed from information provided by the microsome suppliers (BD Gentest) to provide optimal conditions for microsomal enzyme activity. All incubations contained 5 mM $MgCl_2$ and 1 mM NADPH in a final volume of 250 μL buffer (100 mM potassium phosphate buffer, pH 7.4). Test incubations contained drug (prepared from 10 mM stock in DMSO diluted with buffer; final concentration of 2 μM) and pooled male Sprague-Dawley rat liver microsomes possessing cytochrome b_5, CYP3A, CYP2C, CYP 2E1, CYP1A, and CYP4A activity (final protein concentration of 0.5 mg/mL). To control for protein binding, control microsomes derived from a human lymphoblast cell line not possessing detectable cytochrome P450 activity were used. The agent 2-(4-amino-3-methylphenyl)benzothiazole (DF 203), which is known to be metabolized by CYP1A1, was employed as positive control.[20] The incubations were mixed and equilibrated to 37 °C before addition of ice-cold microsomes. After 4 h at 37 °C, incubations were terminated by the addition of three volumes of cold acetonitrile. Following centrifugation for 15 min at 17000*g* the supernatants were filtered and stored at −20 °C until analysis. Samples (25 μL) were analyzed by reverse-phase HPLC on a Hypersil 5 μm C18 (octadecylsilane), 150 mm × 4.6 mm column using the same mobile phase conditions and instrumentation as described for drug stability assays except for a 1 mL/min flow rate and 15 min run time.

Flow Cytometric Assessment of Drug Uptake. A quality control check was performed before each experiment to monitor instrument alignment for the flow cytometer using FlowCheck beads according to the manufacturer's instructions. A549 or MCF-7 cells were grown to approximately 70% confluence in tissue culture flasks (75 cm^2), harvested with trypsin-EDTA solution, collected in culture medium containing 10% fetal bovine serum, centrifuged at 370*g* for 5 min, resuspended in serum-free RPMI medium, aliquotted into flow cytometry tubes (Beckman Coulter), and equilibrated at 37 °C (5% CO_2 incubator) or at 4 °C for 15 min. An aliquot was analyzed on a Coulter Epics XL-MCL flow cytometer using Expo32 software. Data were collected in list mode format for forward and side scatter, and fluorescence emission was collected in the FL2 channel (for **4**, **5**, and **17**; emission wavelength of 575 nm) or the FL3 channel (for **6**; emission wavelength of 620 nm) (excitation wavelength of 488 nm for all agents). The fluorescence detection sensitivity was adjusted so that the drugfree sample fluorescence histogram was below the first log. The cells were gated on the forward scatter against side scatter plot to contain at least 80% of all cells where the density of the plot was greatest to minimize the inclusion of dead or early apoptotic cells or debris. The mean fluorescence for at least 5000 events was recorded. This protocol was then used for all aliquots analyzed. Compound **4** at 37 or 4 °C was added to the cell suspension aliquots at the respective temperatures to a final concentration of 1 μM. After incubation for the desired period (ranging from 30 min to 6 h), the cells were analyzed as above. For the cells incubated at 37 °C, fluorescence was recorded for triplicate samples at each time point and the mean value was calculated. An increase in fluorescence over time was interpreted as uptake of the naturally fluorescent drug by the cells. The negative control was cell aliquots incubated under the same conditions with no drug present. These showed no increase in fluorescence over time. At least two independent experiments were performed for each drug and cell line.

Confocal Microscopy To Examine Intracellular Drug Distribution. Cells (2×10^5) (A549 or MCF7) were grown in 35 mm glass base polystyrene dishes (Iwaki) containing culture medium for 24 h. Drug was then added to a final concentration of 20 μM. After 24 h of incubation with the drug at 37 °C and 5% CO_2, the cells were viewed by a Leica SP2 confocal laser scanning microscope. Cells were maintained at 37 °C by the use of a heated microscope stage. Images were taken using the 488 nm laser line (excitation wavelength of 488 nm, emission at 530−570 nm) for **4** and **17** or the 514 nm laser line (excitation at 514 nm, emission at 520−600 nm) for **5** and **6**. A Z stack was taken with images every 1 or 2 μm and displayed as maximum intensity projections of all the slices using the associated Scanware software.

Acknowledgment. The authors thank Cancer Research U.K. for support to the Experimental Cancer Chemotherapy Research Group.

Supporting Information Available: Representative HPLC traces for the decomposition of **5** when incubated with A549 or MCF-7 cells and for the degradation of **17** in tissue culture media. This material is available free of charge via the Internet at http://pubs.acs.org.

References

(1) Missailidis, S.; Modi, C.; Trapani, V.; Laughton, C. A.; Stevens, M. F. G. Antitumor polycyclic acridines. Part 16. Triplex DNA as a target for DNA-binding polycyclic acridine derivatives. *Oncol. Res*. **2005**, *15*, 95−106.

(2) Heald, R. A.; Stevens, M. F. G. Antitumour polycyclic acridines. Palladium(0) mediated syntheses of quino[4,3,2-*kl*]acridines bearing peripheral substituents as potential telomere maintenance inhibitors. *Org*. *Biomol*. *Chem*. **2003**, *1*, 3337−3389.

(3) Stanslas, J.; Hagan, D. J.; Ellis, M. J.; Turner, C.; Carmichael, J.; Ward, W.; Hammonds, T. R.; Stevens, M. F. G. Antitumor polycyclic acridines. 7. Synthesis and biological properties of DNA affinic tetra- and pentacyclic acridines. *J*. *Med*. *Chem*. **2000**, *43*, 1563−1572.

(4) Gowan, S.; Heald, R.; Stevens, M. F. G.; Kelland, L. R. Potent inhibition of telomerase by small-molecule pentacyclic acridines capable of interacting with G-quadruplexes. *Mol*. *Pharmacol*. **2001**, *60*, 981−988.

(5) Heald, R. A.; Modi, C.; Cookson, J. C.; Hutchinson, I.; Laughton, C. A.; Gowan, S. M.; Kelland, L. R.; Stevens, M. F. G. Antitumor polycyclic acridines. 8. Synthesis and telomerase-inhibitory activity of methylated pentacyclic acridinium salts. *J*. *Med*. *Chem*. **2002**, *45*, 590−597.

(6) Molinski, T. F. Marine pyridoacridine alkaloids: structure, synthesis, and biological chemistry. *Chem*. *Rev*. **1993**, *93*, 1825−1838. Alvarez, M.; Salas, M.; Joule, J. A. Marine nitrogen-containing heterocyclic natural products. Structures and synthesis of compounds containing quinoline and/or isoquinoline units. *Heterocycles* **1991**, *32*, 759−794. Alvarez, M. Synthesis of pyridoacridines. *Heterocycles* **1992**, *34*, 2385−2405. Copp, B. R.; Jompa, J.; Tahir, A.; Ireland, C. M. New tetracyclic pyridoacridine alkaloids from the Indonesian Ascidian, *Eusynstyela latericius*. *J*. *Org*. *Chem*. **1998**, *63*, 8024−8126.

(7) Fugman, B.; Steffan, B.; Steglich, W. Necatarone, an alkaloidal pigment from the gilled toadstool *Lactarius necator (Agaricales)*. *Tetrahedron Lett*. **1984**, *25*, 3575−3578. Hilger, C. S.; Fugman, B.; Steglich, W. Synthesis of necatarone. *Tetrahedron Lett*. **1985**, *26*, 5975−5978. Klamann, J.-D.; Fugman, B.; Steglich, W. Alkaloidal pigments from *Lactarius necator* and *L. atroviridis*. *Phytochemistry* **1989**, *28*, 3519−3523.

(8) Weinstein, J. N.; Myers, T. G.; O'Connor, P. M.; Friend, S. H.; Fornace, A. J.; Kohn, K. W.; Fojo, T.; Bates, S. E.; Rubenstein, L. V.; Anderson, N. L.; Buolamwini, J. K.; van Osdol, W. W.; Monks, A. P.; Scudiero, D. A.; Sausville, E. A.; Zaharevitz, D. W.; Bunow, B.; Viswanadhan, V. N.; Johnson, G. S.; Wittes, R. E.; Paull, K. D. An information-intensive approach to the molecular pharmacology of cancer. *Science* **1997**, *275*, 343−349.

(9) Gavathiotis, E.; Heald, R. A.; Stevens, M. F. G.; Searle, M. S. Recognition and stabilization of quadruplex DNA by a potent new telomerase inhibitor: NMR studies of the 2:1 complex of a pentacyclic methylacridinium cation with $d(TTAGGGT)_4$. *Angew*. *Chem*., *Int*. *Ed*. **2001**, *40*, 4749−4751. Gavathiotis, E.; Heald, R. A.; Stevens, M. F. G.; Searle, M. S. Drug recognition and stabilization of the parallel-stranded DNA quadruplex $d(TTAGGGT)_4$ containing the human telomeric repeat. *J*. *Mol*. *Biol*. **2003**, *334*, 25−36.

(10) Hutchinson, I.; McCarroll, A.; Heald, R. A.; Stevens, M. F. G. Synthesis and properties of bioactive 2- and 3-amino-8-methyl-8*H*-quino[4,3,2-*kl*]acridine and 8,13-dimethyl-8*H*-quino[4,3,2-*kl*]-acridinium salts. *Org*. *Biomol*. *Chem*. **2004**, *2*, 220−228.

(11) Read, M.; Harrison, R. J.; Romagnoli, B.; Tanious, F. A.; Gowan, S. M.; Reszka, A. P.; Wilson, W. D.; Kelland, L. R.; Neidle, S. Structure-based design of selective and potent G-quadruplex-mediated telomerase inhibitors. *Proc. Natl. Acad. Sci. U.S.A.* **2001**, *98*, 4844−4849.

(12) Blackburn, E. H. Telomere states and cell fates. *Nature* **2000**, *408*, 53−56.

(13) Neidle, S.; Parkinson, G. Telomere maintenance as a target for anticancer drug discovery. *Nat. Rev*. *Drug Discovery* **2002**, *1*, 383−393.

(14) Monks, A.; Scuderio, D. A.; Johnson, G. S.; Paull, K. D.; Sausville, E. A. The NCI anti-cancer drug screen: a smart screen to identify effectors of novel targets. *Anti-Cancer. Drug Des.* **1997**, *12*, 533−541.

(15) Cheng, M.-K.; Modi, C.; Grindon, C. R.; Stevens, M. F. G.; Laughton, C. A. The development of novel telomerase inhibitors: structure−activity relationships. *Br. J. Cancer* **2003**, *88* (Suppl. 1), SS40 P63.

(16) Ertl, P.; Rohde, B.; Selzer, P. Fast calculation of molecular polar surface area as a sum of fragment-based contributions and its application to the prediction of drug transport properties. *J. Med. Chem.* **2000,** *43*, 3714−3717.

(17) Lipinski, C. A.; Lombardo, F.; Dominy, B. W.; Feeney, P. J. Experimental and computational approaches to estimate solubility and permeability in drug discovery and development settings. *Adv. Drug Delivery Rev.* **2001**, *46*, 3−26.

(18) Yu, L. J.; Matias, J.; Scudiero, D. A.; Hite, K. M.; Monks, A.; Sausville, E.; Waxman, D. J. P450 enzyme expression patterns in the NCI human tumor cell line panel. *Drug Metab. Dispos.* **2001**, *29,* 304−312.

(19) Kuffel, M. J.; Schroeder, J. C.; Pobst, L. J.; Naylor, S.; Reid, J. M.; Kaufmann, S. H.; Ames, M. M. Activation of the antitumour agent aminoflavone (NSC 686288) is mediated by induction of tumour cell cytochrome P450 1A1/1A2. *Mol. Pharmacol*. **2002**, *62*, 143−153.

(20) Chua, M. S.; Kashiyama, E.; Bradshaw, T. D.; Stinson, S. F.; Brantley, E.; Sausville, E. A.; Stevens, M. F. G. Role of CYP1A1 in modulation of antitumor properties of the novel agent 2-(4-amino-3-methylphenyl)benzothiazole (DF 203, NSC 674495) in human breast cancer cells. *Cancer Res.* **2000**, *60,* 5196−5203.

(21) Cairns, D. *Essentials of Pharmaceutical Chemistry*; Pharmaceutical Press: London, U.K., 2000.

(22) Sadava, D. E. *Cell Biology: Organelle Structure and Function;* Jones and Bartlett Publishers: Boston, MA, 1993.

(23) Jacobson, J.; Duchen, M. R.; Heales, S. J. R. Intracellular distribution of the fluorescent dye nonyl acridine orange responds to the mitochondrial membrane potential: implications for assays of cardiolipin and mitochondrial mass. *J. Neurochem.* **2002**, *82,* 224−233.

(24) Vistica, D. T.; Kenney, S.; Hursey, M.; Boyd, M. R. Role of membrane potential in the accumulation of quaternized ellipticenes by human tumour cell lines. *J. Pharmacol. Exp. Ther.* **1996**, *279*, 1018−1025.

(25) Koya, K.; Li, Y.; Wang, H.; Ukai, T.; Tatsuta, N.; Kawakami, M.; Chen, L. B. MKT-077, a novel rhodacyanine dye in clinical trials, exhibits anticarcinoma activity in preclinical studies based on selective mitochondrial accumulation. *Cancer Res.* **1996**, *56*, 538−543.

(26) Cernay, T.; Zimmerman, H. W. Selective photosensitisation of mitochondria by the lipophilic cationic porphyrin POR10. *J. Photochem. Photobiol., B.* **1996**, *34*, 191−196.

(27) Etheridge, K. T.; Banik, S. S. R.; Armbruster, B. N.; Zhu, Y.; Terns, R. M.; Terns, M. P.; Counter, C. M. The nucleolar localization domain of the catalytic subunit of human telomerase. *J. Biol. Chem.* **2002**, *277*, 24764−24770.

(28) Galy, V.; Olivo-Marin, J. C.; Scherthan, H.; Doye, V.; Rascalou, N.; Nehrbass, U. Nuclear pore complexes in the organization of silent telomeric chromatin. *Nature* **2000**, *403*, 108−112.

JM058031Y